

Topological semimetals with antiferromagnetic order in Hubbard model

Garima Goyal¹ and Dheeraj Kumar Singh¹

School of Physics and Materials Science, Thapar Institute of Engineering and Technology, Patiala-147004, Punjab, India

(Dated: April 3, 2023)

We examine the possible existence of Dirac semimetal with magnetic order in two-dimensional system with a nonsymmorphic symmetry by using mean-field theory within the Hubbard model. We locate the region in the spin-orbit coupling vs Hubbard interaction phase diagram, where such a state is stabilized. The edge states for ribbons extending along both the x and y directions are obtained. Then, we comment on the feasibility of such a state when the $SU(2)$ symmetric nature of the Hubbard interaction is considered. Finally, the effects of magnetic field on the Dirac semimetallic states and corresponding edge states are also explored.

I. INTRODUCTION

A significant progress, accomplished in the direction of topological band theories of insulators [1–6] and superconductors [7–12] in the last decade, has inspired parallelly the study of gapless systems with nontrivial topology [13–18]. The crucial band feature of the gapless topological systems, *i.e.*, semimetals is the symmetry-protected band crossing at the Fermi energy [19–26]. There exists a non-zero topological charge associated with the flux of a curvature function such as the Berry curvature along a closed loop in the Brillouin zone enclosing the band-crossing point [27, 28]. These semimetals exhibit a variety of electronic and transport properties including the edge states [24, 29, 30], anomalous Hall effect [28], large thermopower [31] etc., which make them important for a variety of technological applications [32, 33].

Graphene, with a two-sublattice and honeycomb lattice crystal structure, is one of the systems studied extensively for its topological semimetallic state, which is protected by time-reversal (\mathcal{T}) and parity (\mathcal{P}) invariance in the absence of spin-orbit coupling [34–37]. The quasiparticle dispersion, in the vicinity of band crossings at the Fermi level, is linear in all the momentum directions of the Brillouin zone. A linear energy dispersion at the band crossing points or the Dirac points (DP) describes a pseudo-relativistic massless Dirac fermion [26, 38]. However, a small spin-orbit coupling (SOC) can destroy the Dirac cone, which results in an insulating state with a topological origin [1, 14]. Intense effort is underway to search for 2D material systems besides graphene, which can support the symmetry-protected Dirac semimetal (DSM), because of the tunability of the physical properties of two-dimensional systems.

Recent studies [39–41] suggest that the symmetry-protected two-dimensional DSM state may also exist in the presence of SOC unlike in the case of graphene. However, such a DSM state requires the presence of non-symmorphic crystalline symmetries. The two successive symmetry operations, which may be associated with non-symmorphic symmetry, belong to a point group such as rotation about an axis or reflection in a plane together with a fractional Bravais lattice translation [42–44].

DPs can also be stabilized in three-dimensional systems [40, 45]. 3D DSM was proposed earlier in β -cristobalite BiO_2 [26] and experimental signatures were obtained later in materials such as Na_3Bi [46], Cd_3As_2 [47, 48] etc. There are

two routes via which 3D DSMs can be obtained [19]. First, such a state can appear as an intermediate state, when a system is driven across a transition from the trivial to a topological insulating state in the presence of band inversion. Here, the stability of DPs requires inversion symmetry in addition to the time-reversal symmetry and the removal of any of these two symmetries leads to a semimetal with DPs being split into the Weyl points with non-zero Chern number [49–54]. The other route is through the touching of conduction and valence bands at discrete points in the Brillouin zone, where the DPs are protected by the non-symmorphic symmetries of the crystal-space group. 3D DSM state may also exist in the absence of \mathcal{T} or \mathcal{P} with candidate materials suggested to be CuMnAs and CuMnP with an antiferromagnetic order (AFM) [55]. Protection of DPs in 2D DSM state with AFM order, in the presence of glide mirror symmetry consisting of reflection about y - z plane and half translation, was also explored, when both \mathcal{T} and \mathcal{P} are broken [40].

The stability of the 2D DSM state with AFM order requires a rather stringent condition on the orientation of magnetic moments to be fulfilled. Such a state is possible only when the magnetic moments are pointing along the x axis [40]. However, it is yet to be seen if such a state can be realized in a tight-binding model with $SU(2)$ symmetric Hubbard interaction. In this paper, we examine the possible existence of DSM state with AFM order within the Hubbard model in a setting, where both \mathcal{T} and \mathcal{P} are broken, while their combination \mathcal{TP} remains intact. When the magnetic moments are forced to align along the x or y axis, a phase diagram is obtained in the SOC vs interaction parameter space and the corresponding edge states are obtained. The case with full $SU(2)$ symmetry associated with the electronic spin is also examined for the existence of such a state. The consequence of magnetic field on the DPs and the modified edge states is studied.

This paper is organized as follows. Section II describes the one-orbital Hubbard model with second-neighbor SOC in the sublattice basis. With mean-field decoupled Hubbard interaction, the Hamiltonian for magnetic moments pointing in arbitrary directions is presented. Section III discusses the results including a phase diagram in order to identify the region, where DSM with AFM order is stabilized, especially when the magnetic moments are oriented along the x axis. In addition, the edge states for ribbon geometry when the ribbon is oriented either along x or y direction are obtained. We also present results on the consequence of magnetic moments being allowed to orient themselves in accordance with $SU(2)$

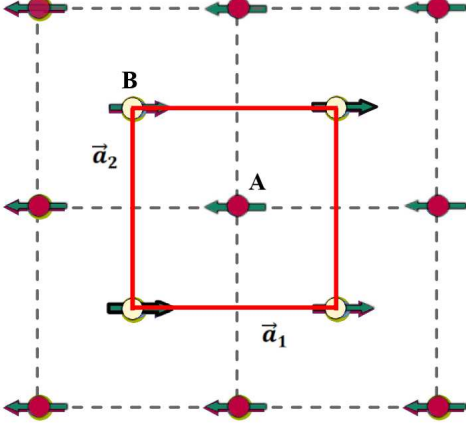


FIG. 1: AFM lattice arrangement with 2 atoms per unit cell (shown in red square) having sublattices A and B with magnetic moments aligned along x -direction whose lattice vectors are $\vec{a}_1 = (1, 0, 0)$ and $\vec{a}_2 = (0, 1, 0)$, respectively. The A(B) atoms are displaced along $+z$ ($-z$) directions by a tiny fraction of the lattice vector to make the crystal non-symmorphic. The red (yellow) circles show the atoms lying above (below) the plane.

symmetry of Hubbard interaction or in the presence of magnetic field. Finally, we present conclusions in section IV.

II. MODEL AND METHOD

In order to study the antiferromagnetic DSM state, we consider a tight-binding Hamiltonian in two-dimension with spin-orbit coupling [1] and Hubbard interaction, which is given by

$$H = t \sum_{\mathbf{i}, \sigma} a_{\mathbf{i}\sigma}^\dagger a_{\mathbf{i}+\delta\sigma} + i\lambda \sum_{\mathbf{i}} \sum_{\sigma\sigma'} \nu_{\mathbf{i}, \mathbf{i}+\delta'} a_{\mathbf{i}\sigma}^\dagger a_{\mathbf{i}+\delta'\sigma'} \sigma_{\sigma\sigma'} + \sum_{\mathbf{i}} U n_{\mathbf{i}\uparrow} n_{\mathbf{i}\downarrow}. \quad (1)$$

The first term represents the delocalization energy gain arising because of hopping of an electron with the spin σ from the site $\mathbf{i} + \delta$ to site \mathbf{i} , where $a_{\mathbf{i}\sigma}^\dagger$ ($a_{\mathbf{i}\sigma}$) is the electron creation (destruction) operator. t is the hopping parameter, which is set to be the unit of energy throughout unless mentioned otherwise. δ is a vector connecting the neighboring sites. Here, only the nearest-neighbor hopping is considered as the second-neighbor hopping will break the particle-hole symmetry, which leads to two DPs appearing at different energies. The second term denotes the next-nearest neighbor SOC whereas the nearest-neighbor SOC is ignored. λ is the SOC parameter and $\nu_{\mathbf{i}, \mathbf{i}+\delta'} = -\nu_{\mathbf{i}+\delta', \mathbf{i}} = \pm 1$ depending on the orientation of two next-nearest neighboring bonds. The third term denotes the onsite Coulomb repulsion between the electrons of opposite spins, where $n_{\mathbf{i}\uparrow} = a_{\mathbf{i}\uparrow}^\dagger a_{\mathbf{i}\uparrow}$.

We consider a square lattice as shown in Fig. 1 with a single orbital per site. The unit cell has two atoms placed in an AFM

arrangement with the lattice vectors denoted by $\vec{a}_1 = (1, 0, 0)$ and $\vec{a}_2 = (0, 1, 0)$, respectively. In order to make the lattice non-symmorphic, the atoms in the unit cell namely A and B are displaced along $+z$ and $-z$ directions, respectively, by a tiny but equal fraction of the lattice vector. This atomic arrangement allows next-nearest-neighbor SOC [14].

The meanfield decoupling of the Hubbard term of the Hamiltonian given by Eq. (1) yields

$$H_{im} = -\frac{U}{2} \sum_{i\sigma} \Psi_i^\dagger (\mathbf{m}_i \cdot \vec{\sigma}) \Psi_i + \frac{U}{4} \sum_i \mathbf{m}_i^2 \quad (2)$$

where $\Psi_i^\dagger = (a_{i\uparrow}^\dagger, a_{i\downarrow}^\dagger)$. The j -th component of magnetic moment at the site i is $m_i^j = \frac{1}{2} \langle \Psi_i^\dagger \sigma^j \Psi_i \rangle$. σ^j is j -th component of Pauli matrices. When incorporated into the sublattice structure of the system with AFM order under consideration, the meanfield decoupled part with broken \mathcal{P} and \mathcal{T} becomes

$$H_{mf} = - \sum_{\mathbf{i}\alpha\beta} \tau a_{\mathbf{i}\alpha}^\dagger (\boldsymbol{\sigma} \cdot \boldsymbol{\Delta})_{\alpha\beta} a_{\mathbf{i}\beta}, \quad (3)$$

where $\boldsymbol{\Delta}$ is the exchange field given by

$$2\boldsymbol{\Delta} = U(m_x \hat{x} + m_y \hat{y} + m_z \hat{z}). \quad (4)$$

m_x , m_y , and m_z represent the components of magnetic moments, which are obtained self consistently. The last term of H_{im} does not appear in H_{mf} as it is a scalar field. $\tau = 1$ on A sublattice and -1 on B sublattice. Thus, after Fourier transforming Eq. 1 and combining it with Eq. 2, the Hamiltonian in the \mathbf{k} -space can be written in the composite sublattice and spin basis as

$$\mathcal{H}(\mathbf{k}) = 4t\tau_1 \cos \frac{k_x}{2} \cos \frac{k_y}{2} + (\Delta_x - 2\lambda \sin k_y) \sigma_1 \otimes \tau_3 + (\Delta_y + 2\lambda \sin k_x) \sigma_2 \otimes \tau_3 + \Delta_z \sigma_3 \otimes \tau_3, \quad (5)$$

where σ and τ are Pauli matrices in the spin and sublattice spaces. The two-fold degenerate eigenvalues of the Hamiltonian can be readily shown to be

$$E_{\mathbf{k}} = \pm \sqrt{\varepsilon_{\mathbf{k}}^2 + \Delta_x'^2 + \Delta_y'^2 + \Delta_z^2}, \quad (6)$$

where $\varepsilon_{\mathbf{k}} = 4t \cos \frac{k_x}{2} \cos \frac{k_y}{2}$, $\Delta_x' = \Delta_x - 2\lambda \sin k_y$, $\Delta_y' = \Delta_y + 2\lambda \sin k_x$. The eigenvector $(\phi_{\mathbf{k}\uparrow}^A, \phi_{\mathbf{k}\uparrow}^B, \phi_{\mathbf{k}\downarrow}^A, \phi_{\mathbf{k}\downarrow}^B)^T$ of the Hamiltonian $\mathcal{H}(\mathbf{k})$ is used to obtain the magnetic moments in a self-consistent manner, where one electron per site is considered throughout. The components of magnetic moment at the sublattice A is

$$\begin{aligned} m_z &= n_{\uparrow}^A - n_{\downarrow}^A \\ &= \sum_{\mathbf{k}, l} (\phi_{\mathbf{k}\uparrow}^{A*} \phi_{\mathbf{k}\uparrow}^A \Theta(E_f - E_{\uparrow, l}) - \phi_{\mathbf{k}\downarrow}^{A*} \phi_{\mathbf{k}\downarrow}^A \Theta(E_f - E_{\downarrow, l})) \\ m_x &= \sum_{\mathbf{k}, l} (\phi_{\mathbf{k}\uparrow}^{A*} \phi_{\mathbf{k}\downarrow}^A + \phi_{\mathbf{k}\uparrow}^A \phi_{\mathbf{k}\downarrow}^{A*}) \Theta(E_f - E_{\uparrow, l}) \Theta(E_f - E_{\downarrow, l}) \\ m_y &= \sum_{\mathbf{k}, l} (-i \phi_{\mathbf{k}\uparrow}^{A*} \phi_{\mathbf{k}\downarrow}^A + i \phi_{\mathbf{k}\uparrow}^A \phi_{\mathbf{k}\downarrow}^{A*}) \Theta(E_f - E_{\uparrow, l}) \\ &\quad \times \Theta(E_f - E_{\downarrow, l}), \end{aligned} \quad (7)$$

where l is the band index.

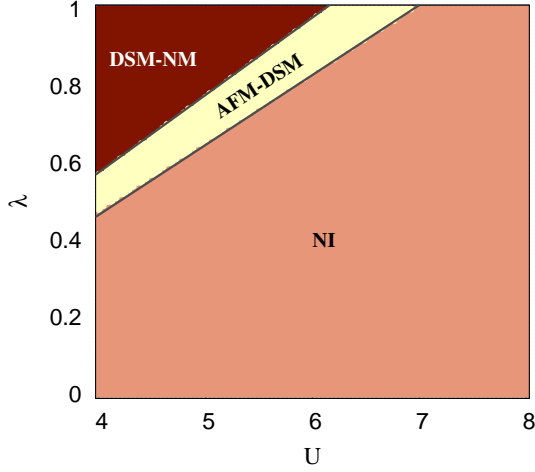


FIG. 2: Phase diagram in the $\lambda - U$ space in the range $4 \leq U \leq 8$ and $0 \leq \lambda \leq 1.0$ at half-filling ($n = 1.0$). DSM state with AFM order is obtained only for a very narrow range of λ which separates the DSM state without magnetic order (DSM-NM) and the normal insulating state (NI).

III. RESULTS

The energy dispersion given by Eq. 4 is gapped whenever the magnetic moments have a component along z direction or along a direction in the x - y plane other than x or y axes. However, there exists a two-fold degenerate band crossing at $E_k = 0$ provided that the magnetic moments are oriented either along x or y direction. In these cases, the energy dispersions are linear in the vicinity of the band crossing which indicates that these crossing points are DPs. These DPs are protected by glide mirror symmetry $\{M_{\hat{x}}|\frac{1}{2}0\}$ and $\{M_{\hat{y}}|0\frac{1}{2}\}$ depending on whether the magnetic moments are oriented along x and y , respectively [40].

Fig. 2 shows the self-consistently obtained phase diagram in the λ - U parameter space when the magnetic moments are aligned along the x direction. Three different phases are obtained; DSM without magnetic order, DSM with AFM order, and a normal insulator. The DSM state with AFM order is obtained only for a very narrow window of SOC centered around $\lambda \sim 0.8$, which is sandwiched in between the DSM state without magnetic ordering and the normal insulating state (NI). The DPs occur at the momenta $\mathbf{k} = (\pi, k_{y0})$ and $(\pi, \pi - k_{y0})$ with $\sin k_{y0} = \Delta_x/2\lambda$ [40]. Therefore, whenever the self-consistently obtained exchange field satisfies the condition $0 < \Delta_x < 2\lambda$, the DSM state with AFM order is obtained.

Fig. 3 shows the electronic dispersion in the three phases for a fixed Coulomb interaction parameter $U = 5.0$ and different values of SOC parameter λ . In Fig. 3(a), the bulk dispersion is obtained for $\lambda = 0.4$ corresponding to the normal insulating state with AFM order indicated by a gap opening at the Fermi level. The gap opening disappears when SOC is increased and two DPs appear along X_1 -M but they are located away from the high-symmetry points X_1 and M (Fig. 3(b)). The energy dispersion in the vicinity of DPs can be obtained from Eq. (4),

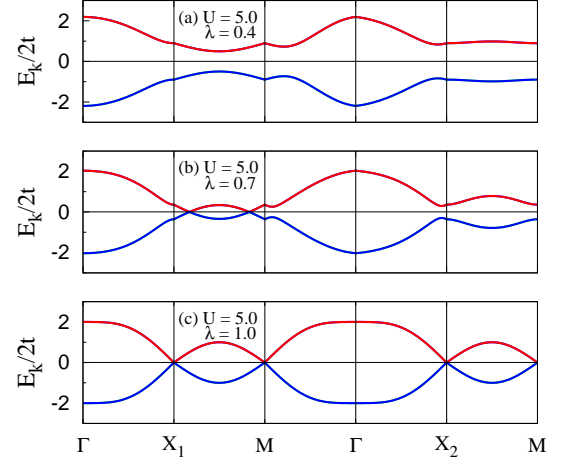


FIG. 3: For $U = 5$, electronic dispersions are plotted when (a) $\lambda = 0.4$, (b) $\lambda = 0.7$ and (c) $\lambda = 1.0$. For these three different values, normal insulator, DSM state with antiferromagnetic order and without any magnetic order are obtained, respectively. In each case, the DPs are protected by the non-symmorphic symmetries.

which is

$$E_k = \pm 2\sqrt{(\lambda^2 + t^2 \cos^2 k_{y0}/2)q_x^2 + (\lambda^2 \cos^2 k_{y0})q_y^2}. \quad (8)$$

These DPs are protected by glide mirror plane symmetry $\{M_{\hat{x}}|\frac{1}{2}0\}$ while the dispersion in their vicinity is independent of magnetic moment. For $\lambda = 1.0$ (Fig. 3(c)), the magnetic moment vanishes, therefore, three DPs are obtained at the time-reversal invariant momenta, *i.e.*, $X_1(\pi, 0)$, $M(\pi, \pi)$ and $X_2(0, \pi)$ of the Brillouin-zone boundary. These DPs are protected by either of the screw axes $\{C_{2\hat{x}}|\frac{1}{2}0\}$ and $\{C_{2\hat{y}}|0\frac{1}{2}\}$ or by glide mirror plane symmetry $\{M_{\hat{z}}|\frac{1}{2}\frac{1}{2}\}$ as the system has now both \mathcal{T} and \mathcal{P} symmetry intact in the absence of any magnetic moment [14].

The edge states, in the topological insulators, are pairs of states with opposite spins propagating in directions opposite to each other. The dispersion of the edge state crosses the Fermi level and appears as a bridge between the bands corresponding to valence and conduction electrons. They are also supported in systems such as Dirac and Weyl semimetals. There are numerous examples including the localized flat edge states in the quasi-one-dimensional graphene ribbons of zigzag shape [56–59]. While the edge states in graphene are attributed to the Dirac cones, these states may even be found in their absence when degeneracy occurs at high symmetry points [60–62]. Recent studies have explored the edge states in the Weyl semimetals without any magnetic order when the time-reversal symmetry is broken in the nonsymmorphic system [41].

Here, we examine the edge-state dispersion in the Dirac semimetallic state with AFM order in quasi-one dimensional system. It may be noted that the nature of the edge state may depend on how the in-plane magnetic moments are oriented with respect to the ribbon length, as the four-fold rotation symmetry is broken. First, we consider a ribbon of width W

lying along the y direction so that k_y becomes a good quantum number. The ribbon Hamiltonian H_{Rby} with dimension $2W \times 2W$, where W is the number of atomic chains in the ribbon, is given by

$$H_{Rby}(\mathbf{k}) = \begin{pmatrix} H_{1+} & H_2 & H_3 & O & \cdots \\ H_2^\dagger & H_{1-} & H_2 & H_3 & \cdots \\ H_3^\dagger & H_2^\dagger & H_{1+} & H_2 & \cdots \\ O & H_3^\dagger & H_2^\dagger & H_{1-} & \cdots \\ \vdots & \vdots & \vdots & \vdots & \ddots \end{pmatrix}, \quad (9)$$

where

$$H_{1\pm} = \begin{pmatrix} 0 & \pm(-2\lambda \sin k_y + \Delta_x) \\ \pm(-2\lambda \sin k_y + \Delta_x) & 0 \end{pmatrix},$$

$$H_2 = \begin{pmatrix} 2t \cos(k_y/2) & 0 \\ 0 & 2t \cos(k_y/2) \end{pmatrix}$$

and

$$H_3 = \begin{pmatrix} 0 & -\lambda \\ \lambda & 0 \end{pmatrix}.$$

$H_{1\pm}$ is the element in a matrix form of Hamiltonian corresponding to a chain while H_2 and H_3 matrices connect a chain to the nearest and the next-nearest neighbor chains.

Fig. 4 shows the edge states obtained for three different cases when the number of chains is even. The results are same also for an odd number of chains. In the DSM state without AFM order, when the Hubbard interaction $U = 0$, the edge states cross the Fermi energy at $k_y = 0, \pi$ and 2π . However, in the DSM state with AFM order, the crossing points shift away towards a point in between $k_y = 0$ and π . There exists a special U_s for a given value of λ , where the crossing coincides. Beyond that U_s , *i.e.* in the insulating state, there are no states crossing the Fermi energy, indicating the appearance of a normal insulator.

Next, we consider a ribbon of width W lying along the x -direction. The Hamiltonian matrix corresponding to this ribbon also has size $2W \times 2W$ and it is given by

$$H_{Rbx}(\mathbf{k}) = \begin{pmatrix} H'_{1+} & H'_2 & H'_3 & O & \cdots \\ H'^{\dagger}_2 & H'_{1-} & H'_2 & H'_3 & \cdots \\ H'^{\dagger}_3 & H'^{\dagger}_2 & H'_{1+} & H'_2 & \cdots \\ O & H'_3 & H'^{\dagger}_2 & H'_{1-} & \cdots \\ \vdots & \vdots & \vdots & \vdots & \ddots \end{pmatrix}, \quad (10)$$

where

$$H'_{1\pm} = \begin{pmatrix} 0 & \pm(-2i\lambda \sin k_x + \Delta_x) \\ \pm(-2i\lambda \sin k_x + \Delta_x) & 0 \end{pmatrix},$$

$$H'_2 = \begin{pmatrix} 2t \cos(k_x/2) & 0 \\ 0 & 2t \cos(k_x/2) \end{pmatrix}$$

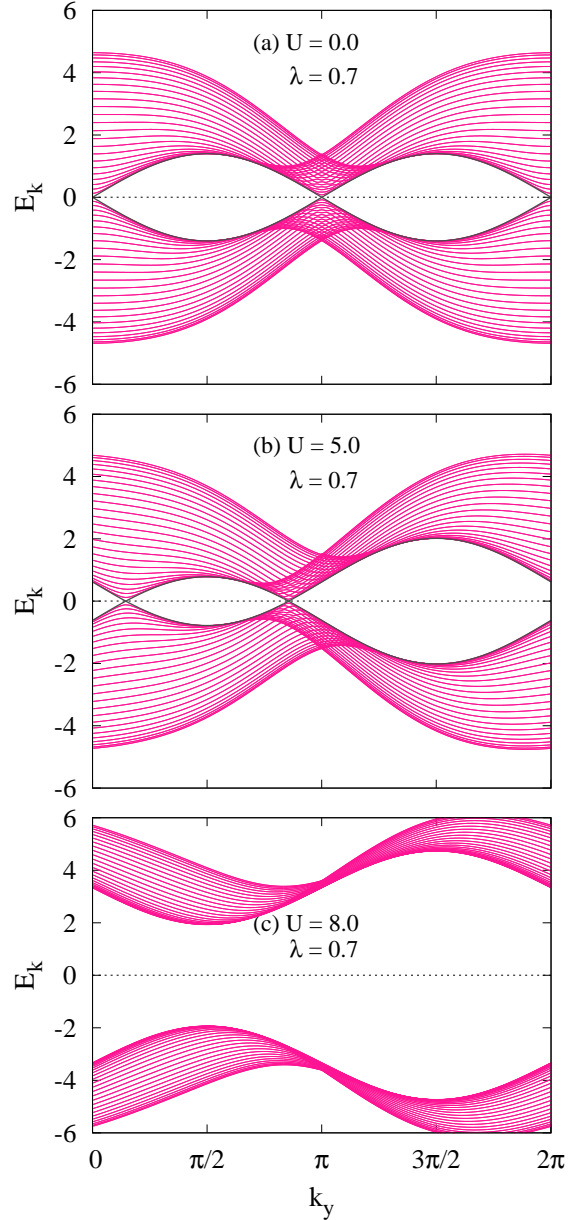


FIG. 4: Edge-state dispersions and bulk bands for a ribbon of width $W = 50$ lying along y direction and projected onto one dimensional Brillouin zone for $\lambda = 0.7$ and (a) $U = 0.0$, (b) 5.0 and (c) 8.0 . The edge-state dispersion crosses each other at the same points as the bulk bands at the Fermi level and disappear beyond U_s , which indicates appearance of a normal insulator.

and

$$H'_3 = \begin{pmatrix} 0 & i\lambda \\ i\lambda & 0 \end{pmatrix}.$$

$H'_{1\pm}$, H'_2 and H'_3 are matrices as described before except that now they are part of Hamiltonian for a ribbon oriented along x axis.

Fig. 5 shows the edge states obtained when the chains as well as the magnetic moments are oriented along the x direction. In the DSM state without any AFM order, the nature of

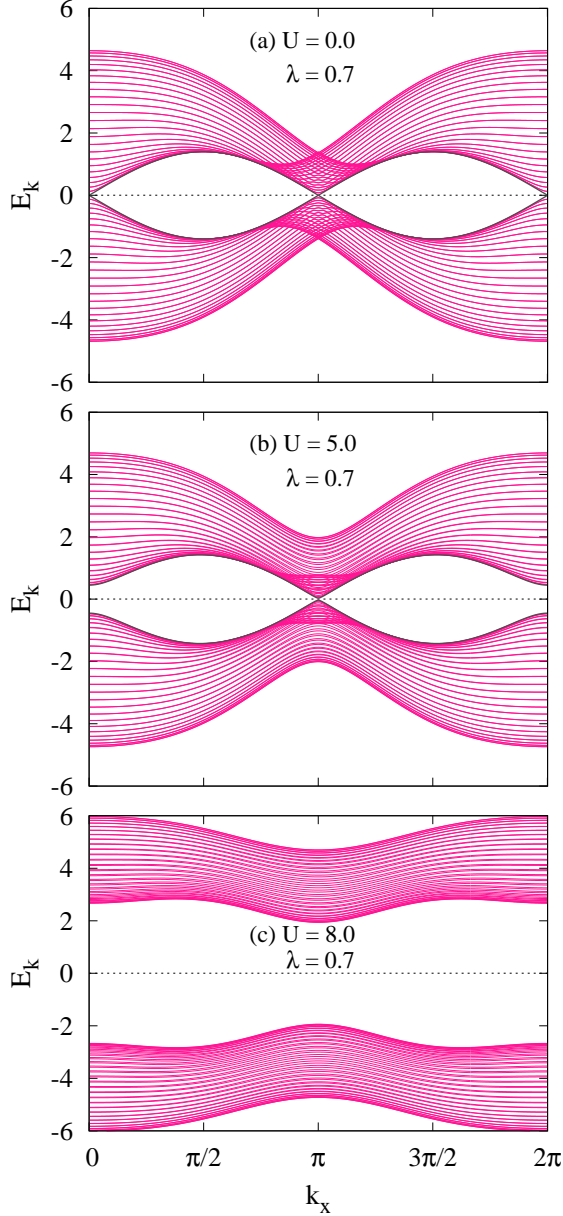


FIG. 5: Edge-state dispersions for a ribbon of width $W = 50$ oriented along x direction compared to the bulk bands, which are projected onto one dimensional Brillouin zone for $\lambda = 0.7$ and (a) $U = 0.0$, (b) 5.0 and (c) 8.0.

the edge state, as expected, is the same as the case when the ribbon was oriented along the y axis. However, we find that the edge state crosses the Fermi level at $k_x = \pi$ in the DSM state with AFM order. The location of the crossing does not change upon increasing U , which is not unusual as the DPs are found along high-symmetry direction for $k_x = \pi$ although the size of the magnetic moments increases with interaction. Finally, the crossing disappears at U_s and beyond.

Thus far, we have presented the results of our calculations for the case when the magnetic moments are forced to align along x . Next, we allow the magnetic moments to pick

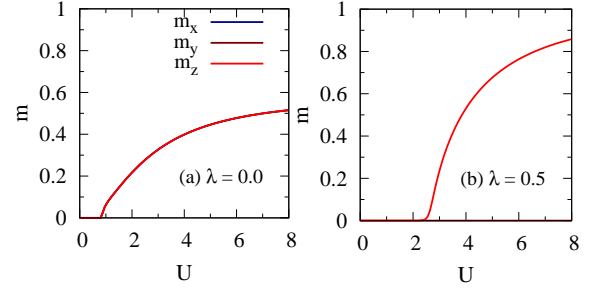


FIG. 6: Self-consistently obtained components of magnetic moments when the system is allowed to have all the components in the (a) absence and (b) presence of SOC. When $\lambda = 0$, all the components are non-zero and equal, the corresponding curves are coinciding. For $\lambda \neq 0$, $m_x = m_y = 0$ and $m_z \neq 0$ is non-zero.

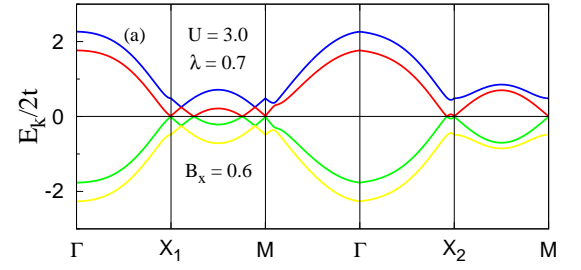


FIG. 7: Electronic dispersion is plotted along the high symmetry directions (a) when the magnetic field is applied along the x axis for the parameters $U = 3.0$, $\lambda = 0.7$, and $B_x = 0.6$. The Dirac points are split into Weyl nodes along X_1 -M and an additional pair of Weyl nodes emerge along Γ - X_2 as a result of perturbation.

up an arbitrary direction in the self-consistent scheme, *i.e.*, m_x , m_y , and m_z are set initially to be non-zero. The results obtained this way are shown in Fig. 6. In the absence of second-neighbor SOC, all the magnetic components have the same value in accordance with $SU(2)$ symmetry as the Hamiltonian has continuous spin-rotation symmetry. However, $SU(2)$ symmetry of the Hamiltonian is lost on the inclusion of spin-orbit coupling, and the magnetic moments are preferably aligned out of the plane as the in-plane components of magnetic moments $m_x = m_y = 0$. Thus, a Dirac semimetal with AFM order, as it appears, may not be feasible.

Next, we address the question of whether a semimetallic state can be stabilized in the presence of a magnetic field. A magnetic field applied along the positive x axis may support the AFM order with magnetic moments along the x axis. However, it also breaks the symmetry \mathcal{PT} effected by $i\sigma_y\mathcal{K}\tau_1$ while retaining the symmetry $\{M_{\hat{x}}|\frac{1}{2}0\}$, where \mathcal{K} is the complex conjugation operator. The consequence of magnetic field on the electronic dispersion can be obtained by incorporating the term

$$\mathcal{H}_m = B_x \sigma_x \otimes \tau_0 \quad (11)$$

into the Hamiltonian (Eq. (3)), where B_x is the magnetic-field

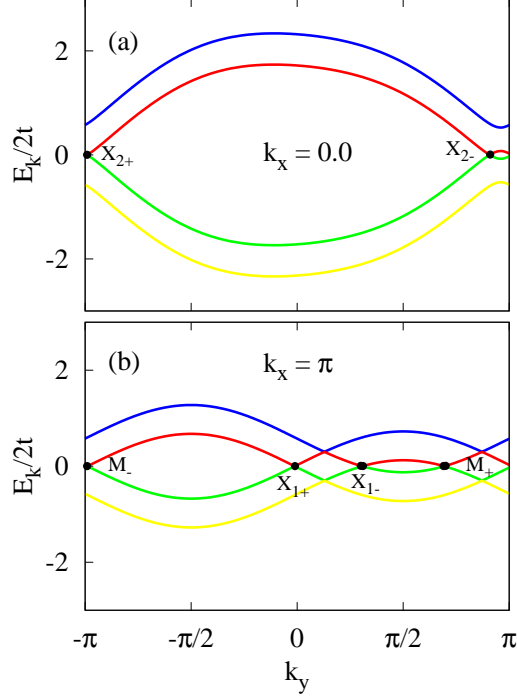


FIG. 8: To highlight the Weyl points, the dispersion in Fig 7 is re-plotted for (a) $k_x = 0$ and (b) $k_x = \pi$ separately when k_y is varied from $-\pi$ to π . In addition to the two DPs, which are split into two Weyl points, an additional pair of Weyl points may also be noticed.

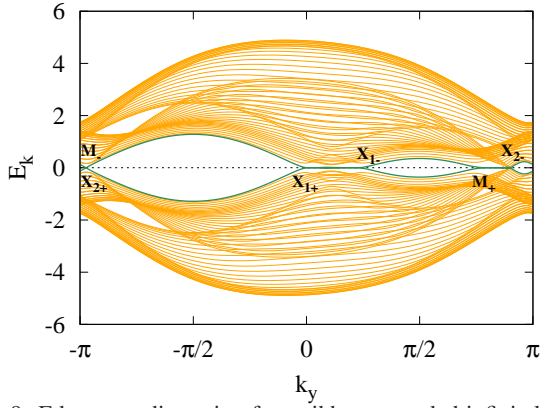


FIG. 9: Edge-state dispersion for a ribbon extended infinitely along y direction and having a finite width $W = 50$ in the presence of magnetic field. The parameters are $U = 3.0$, $\lambda = 0.7$, and $B_x = 0.6$.

intensity. Then, the electronic dispersion is given by

$$E_{\mathbf{k}} = \pm \sqrt{\pm 2 \sqrt{B_x^2(\varepsilon_{\mathbf{k}}^2 + \Delta_{x\mathbf{k}}^2) + B_x^2 + \varepsilon_{\mathbf{k}}^2 + \Delta_{x\mathbf{k}}'^2 + \Delta_{y\mathbf{k}}'^2} + \Delta_z^2}. \quad (12)$$

It is plotted in Fig. 7 for self-consistently obtained antiferromagnetically ordered state for $U = 3.0$, $\lambda = 0.7$ and $B_x = 0.6$. Note that the magnetic moments are allowed to choose any direction in the self-consistent scheme and they

choose x direction for the above set of parameters. All the three DPs in the presence of any exchange and magnetic field are split into Weyl points. One pair of Weyl points $X_{2\pm}$ are located along $k_x = 0$ at k_{y0} determined by the condition

$$16 \cos^2 k_y/2 + (\Delta_x - 2\lambda \sin k_y)^2 = B_x^2 \quad (13)$$

provided that the solution exists. On the other hand, two pairs of Weyl points $X_{1\pm}$ and $M_{2\pm}$ are found at k_{y0} s given by $k_{y0} = \arcsin(\pm B_x + \Delta_x)/2\lambda$ and $k_{y0} = \pi - \arcsin(\pm B_x + \Delta_x)/2\lambda$ along X_1 -M for $k_x = \pi$ (Fig. 8(a) and (b)). The Weyl points along $k_x = 0$ and π are accidental as they are not protected by any symmetry, particularly, the nonsymmorphic symmetry $\{C_{2y}|0\frac{1}{2}\}$ is already broken. Whether the DPs are split into Weyl points or the state turns into a normal insulator is determined by the Hubbard on-site interaction U . The Weyl semimetal is stabilized, when U is small and the magnetic field is comparable to SOC, which forces the magnetic moments to orient along the x direction while considering the $SU(2)$ symmetry of Hubbard interaction. Moreover, the accidental degeneracy expected to occur along X_2 -M in the absence of AFM order is absent [41]. Formation of Weyl points is accompanied by the edge states, which are shown in Fig. 9 for a ribbon of infinite length along the y axis and having a finite width $W = 50$ along x axis. The edge states are the projections of the Weyl points which are accompanied by the flat bands connecting the Weyl nodes with opposite Chern numbers. They are distinctly seen to be present for each pair of Weyl points.

Here, we focused on the role of interaction in stabilizing magnetically ordered topological semimetallic state within one-band Hubbard model at half filling. In particular, we showed that such a state is realized when an in-plane magnetic field is applied along $(1, 0)$ or $(0, 1)$ direction. The consequence of band fillings other than half, presence of more than one orbital, and nearest-neighbor spin-orbit coupling are issues of significant interest which we discuss below.

IV. DISCUSSION

In the current work, the second-neighbor spin-orbit coupling was considered instead of the first-neighbor [26]. As originally proposed, the topologically-protected DSM state may exist in a non-magnetic state when the second-neighbor spin-orbit coupling and the nonsymmorphic symmetry are present. It may be noted that the direction of magnetic moments depends on the nature of spin-orbit coupling. The self-consistently obtained magnetic moments, with the $SU(2)$ symmetric on site interaction, are oriented in plane when only the first-neighbor spin-orbit coupling is considered in contrast to their out of plane alignment when only the second-neighbor spin-orbit coupling is considered. It may also be noted that a gap is opened at the Fermi level for half filling in the case of former.

A magnetically ordered DSM state within the Hubbard model exists only when two of the four bands ($n = 2$) are completely filled and the spin arrangement is of checkerboard type. Not much is known about a magnetically ordered DSM

state for other band fillings. A recent work suggests that a DSM state with stripe-like magnetic order and integer band fillings other than $n = 2$ can also be realized. The band filling $n = 6$, i. e., six out of eight bands are completely filled. While $n = 2$ corresponds to one electron per site in the checkerboard case, $n = 6$ for stripe order corresponds to an average electronic occupancy of three-quarter for each site [63]. It will be interesting to see whether the DSM state with striped magnetic order in presence of both the first- and second-neighbor spin-orbit coupling is stable when the $SU(2)$ symmetric on site Coulombic interaction is incorporated in self-consistent mean-field theory.

The DSM state in the multi-band correlated electron system is of strong current interest and the existence of DPs have been reported in a variety of system though often far from the Fermi surface. A large volume of studies have focused on the electronic-band structure and system without any magnetic order. However, one widely studied multi-orbital system with moderate correlations is iron pnictide, which exhibits a striped spin-density wave (SDW) order. The DPs in the SDW state of iron pnictides are not far away from the Fermi level and they are believed to play an important role in the transport properties. Although the symmetries which protect the DPs are different. In particular, the stability of the Dirac cones and nodes in the SDW state without any nonsymmorphic symmetry is a consequence of three symmetries, (i) collinear arrangement of magnetic moments, (ii) inversion symmetry about any iron atom, and combined time reversal and inversion of magnetic moments [50]. Since the the DPs are not far away from the Fermi surface, there is a possibility of tuning the location

of these DPs by parameters such orbital-splitting by applying mechanical pressure [64].

V. CONCLUSION

To conclude, we have examined the possible existence of Dirac semimetallic state with AFM ordering within one-orbital Hubbard model with second-neighbor spin-orbit coupling and nearest-neighbor hopping. In the non-symmorphic symmetry, when the magnetic moments are directed along the x axis in the antiferromagnetic arrangement, we obtain the phase diagram in the interaction vs spin-orbit coupling parameter space. The nature of edge states is uncovered for different relative orientations of magnetic moments with respect to ribbon geometry. Our findings also suggest that the Dirac semimetallic state with AFM order may not exist when $SU(2)$ symmetry of the on-site interaction is taken into account. On the other hand, Weyl semimetal is stabilized when magnetic field is applied along a direction same as that of magnetic moments.

ACKNOWLEDGEMENTS

D.K.S. was supported through DST/NSM/R&D_HPC_Applications/2021/14 funded by DST-NSM and start-up research grant SRG/2020/002144 funded by DST-SERB.

-
- [1] C. L. Kane and E. J. Mele, Phys. Rev. Lett. **95**, 226801 (2005).
 - [2] M. Z. Hasan and C. L. Kane, Rev. Mod. Phys. **82**, 3045 (2010).
 - [3] M. Nakahara, Geometry, Topology and Physics, CRC Press, (2003).
 - [4] L. Fu, C. L. Kane, and E. J. Mele, Phys. Rev. Lett. **98**, 106803 (2007).
 - [5] B. A. Bernevig and S. C. Zhang, Phys. Rev. Lett., **96**, 106802 (2006).
 - [6] F. D. M. Haldane, Phys. Rev. Lett. **61**, 2015 (1988).
 - [7] X.-L. Qi and S.-C. Zhang, Mod. Rev. Phys. **83**, 1057 (2011).
 - [8] A. Bansil, H. Lin, and Tanmoy Das, Rev. Mod. Phys. **88**, 021004 (2016).
 - [9] B. A. Bernevig and T. L. Hughes, Topological insulators and topological superconductors (Princeton University Press, 2013).
 - [10] A. P. Schnyder, S. Ryu, A. Furusaki, and A. W. W. Ludwig, Phys. Rev. B **78**, 195125 (2008).
 - [11] A. Kitaev, AIP Conf. Proc. **1134**, 22 (2009).
 - [12] X. L. Qi, T. L. Hughes, S. Raghu, and S. C. Zhang, Phys. Rev. Lett. **102**, 187001 (2009).
 - [13] O. Deb *et al.*, J. Phys.: Condens. Matter **26**, 315009 (2014).
 - [14] C. Kane and E. Mele, Phys. Rev. Lett. **95**, 146802 (2005).
 - [15] R. Roy, Phys. Rev. B **79**, 195322 (2009).
 - [16] C. Xu and J. E. Moore, Phys. Rev. B **73**, 064417 (2006).
 - [17] Y. Xia, L. Wray, D. Qian, D. Hsieh, A. Pal, H. Lin, A. Bansil, D. Grauer, Y. Hor, R. Cava, and M. Hasan, Nat. Phys. **5**, 398 (2009).
 - [18] C. Wu, B. A. Bernevig, and S. C. Zhang, Phys. Rev. Lett. **96**, 106401 (2006).
 - [19] B.-J. Yang and N. Nagaosa, Nat. Commun. **5**, 4898 (2014).
 - [20] H. Weng, C. Fang, Z. Fang, B. A. Bernevig, and X. Dai, Phys. Rev. X **5**, 011029 (2015).
 - [21] H. Weng, X. Dai, and Z. Fang, J. Phys. Condens. Matter **28**, 303001 (2016).
 - [22] C. Fang, H. Weng, X. Dai, and Z. Fang, Chin. Phys. B **25**, 117106 (2016).
 - [23] B. Yan and C. Felser, Annu. Rev. Condens. Matter Phys. **8**, 337 (2017).
 - [24] N. Armitage, E. Mele, and A. Vishwanath, Rev. Mod. Phys. **90**, 015001 (2018).
 - [25] H. Gao, J. W. Venderbos, Y. Kim, and A. M. Rappe, Annu. Rev. Mater. Sci. **49**, 153 (2019).
 - [26] S. M. Young, S. Zaheer, J. C. Teo, C. L. Kane, E. J. Mele, and A. M. Rappe, Phys. Rev. Lett. **108**, 140405 (2012).
 - [27] M. V. Berry, Proc. R. Soc. Lond. A **392**, 45–57 (1984).
 - [28] A. Burkov, Annu. Rev. Condens. Matter Phys. **9**, 359 (2018).
 - [29] A. A. Burkov, Nat. Mater. **15**, 1145 (2016).
 - [30] P. Li, W. Wu, Y. Wen, C. Zhang, J. Zhang, S. Zhang, Z. Yu, S. A. Yang, A. Manchon, and X.-X. Zhang, Nat. Commun. **9**, 3990 (2018).
 - [31] X. Huang, L. Zhao, Y. Long, P. Wang, D. Chen, Z. Yang, H. Liang, M. Xue, H. Weng, Z. Fang, X. Dai, and G. Chen, Phys. Rev. X **5**, 031023 (2015).
 - [32] P. Liu, J.R. Williams, and J.J. Cha, Nat. Rev. Mater. **4**, 479 (2019).

- (2019).
- [33] R. Lundgren, P. Laurell, and G.A. Fiete, *Phys. Rev. B* **90**, 165115 (2014).
 - [34] A. H. Castro Neto, F. Guinea, N. M. R. Peres, K. S. Novoselov, and A. K. Geim, *Rev. Mod. Phys.* **81**, 109 (2009).
 - [35] K. S. Novoselov, A. K. Geim, S. V. Morozov, D. Jiang, M. I. Katsnelson, I. V. Grigorieva, S. V. Dubonos, and A. A. Firsov, *Nature (London)* **438**, 197 (2005).
 - [36] A. H. C. Neto, N. M. R. Peres, K. S. Novoselov, and A. K. Geim, *Rev. Mod. Phys.* **81**, 109 (2009).
 - [37] S. Zhou, G. H. Gweon, J. Graf, *et al.*, *Nat. Phys.* **2**, 595–599 (2006).
 - [38] Z. Wang, Y. Sun, X.-Q. Chen, C. Franchini, G. Xu, H. Weng, X. Dai, and Z. Fang, *Phys. Rev. B* **85**, 195320 (2012).
 - [39] S. M. Young and C. L. Kane, *Phys. Rev. Lett.* **115**, 126803 (2015).
 - [40] J. Wang, *Phys. Rev. B* **95**, 115138 (2017).
 - [41] P. G. Matveeva, D. N. Aristov, D. Meidan, D. B. Gutman, *Phys. Rev. B* **99**, 075409 (2019).
 - [42] B. J. Wieder and C. L. Kane, *Phys. Rev. B* **94**, 155108 (2016).
 - [43] Y. X. Zhao and A. P. Schnyder, *Phys. Rev. B* **94**, 195109 (2016).
 - [44] C. J. Bradley and A. P. Cracknell, *The Mathematical Theory of Symmetry in Solids*, Clarendon Press Oxford, (1972).
 - [45] Z. Wang, H. Weng, Q. Wu, X. Dai, and Z. Fang, *Phys. Rev. B* **88**, 125427 (2013).
 - [46] Z. K. Liu *et al.*, *Science* **343**, 864 (2014).
 - [47] Z. K. Liu *et al.*, *Nat. Mater.* **13**, 677 (2014).
 - [48] S. Borisenko, Q. Gibson, D. Evtushinsky, V. Zabolotnyy, B. Büchner, and R. J. Cava, *Phys. Rev. Lett.* **113**, 027603 (2014).
 - [49] S. Murakami, *New J. Phys.* **9**, 356 (2007).
 - [50] X. Wan, A. M. Turner, A. Vishwanath, and S. Y. Savrasov, *Phys. Rev. B* **83**, 205101 (2011).
 - [51] G. Xu, H. Weng, Z. Wang, X. Dai, and Z. Fang, *Phys. Rev. Lett.* **107**, 186806 (2011).
 - [52] A. A. Burkov and L. Balents, *Phys. Rev. Lett.* **107**, 127205 (2011).
 - [53] Y. X. Su *et al.*, *Science* **349**, 613 (2015).
 - [54] B. Q. Lv *et al.*, *Phys. Rev. X* **5**, 031013 (2015).
 - [55] P. Tang *et al.*, *Nat. Phys.* **12**, 1100–1104 (2016).
 - [56] K. Nakada, M. Fujita, G. Dresselhaus, and M. S. Dresselhaus, *Phys. Rev. B* **54**, 17954 (1996).
 - [57] M. Fujita, K. Wakabayashi, K. Nakada, and K. Kusakabe, *J. Phys. Soc. Japan* **65**(7), 1920 (1996).
 - [58] K. Wakabayashi, M. Fujita, H. Ajiki, and M. Sigrist, *Phys. Rev. B* **59**(12), 8271 (1999).
 - [59] K. Wakabayashi, K. Sasaki, T. Nakanishi, and T. Enoki, *Sci Technol. Adv. Mate.* **11**, 5 (2010).
 - [60] H. A. Fertig, L. Brey, *Phys. Rev. Lett.* **97** (2006) 116805.
 - [61] A. Lau and C. Timm, *Phys. Rev. B* **88** 165402 (2013)
 - [62] J. L. Lado, N. García-Martínez, and J. Fernández-Rossier, *Synth Met.* **210**, 56-67 (2015).
 - [63] S. M. Young and B. J. Wieder, *Phys. Rev. Lett.* **118**, 186401 (2017).
 - [64] G. Goyal and D. K. Singh, arXiv:2207.04365.
 - [65]